JOURNAL OF MATERIALS SCIENCE 35 (2000) 1845–1855

Evaluation of the mechanical performance of zirconia bioceramic based on the size of incipient flaw

B. J. HULM, J. D. PARKER
Department of Materials Engineering, University of Wales, Swansea, SA2 8PP
E-mail: b.j.hulm@swansea.ac.uk

The mechanical performance of ceramic materials is highly dependent on the existence of incipient flaws. This paper investigates the relationship between the size of the pre-existing flaw and failure stress for disc-shaped specimens of zirconia bioceramic subjected to an equibiaxial stress field. As the size of initiating flaw increased, the stress under which discs failed decreased, sensibly allowing the fracture toughness of the material to be calculated. The value obtained, 8 $MPam^{1/2}$, is in reasonable agreement with previous experience, giving confidence in the validation procedure used and the data obtained. For cyclic loading, periods of stable fatigue crack growth occurred with initial defects extending to reach critical values. Based on data for discs that failed under monotonic loading conditions, it was possible to determine the critical flaw size and hence degree of crack growth necessary for discs to fail from fatigue at a given peak cyclic stress. Predictive constant flaw size fatigue curves showed reasonable accuracy in that the estimated incipient flaw size at a given fatigue life was equivalent to the true flaw size, measured from the fracture surface of failed disc specimens.

1. Introduction

There is an increasing awareness of the potential advantages ceramics display over other materials for engineering applications. Due to high wear resistance, chemical stability and the ability to retain mechanical strength at high temperatures, ceramics are currently used, or being considered, for a range of demanding applications. Such applications include inserts for cutting tools, bearings, valves, thermal barrier coatings, high temperature components in gas turbine engines and articulating implant materials. Despite attractive chemical and mechanical properties, traditionally ceramics are brittle, with poor impact resistance and low flaw tolerance. However, critical improvements in processing techniques have resulted in important advances in the properties of these materials, most notably the fracture toughness, allowing a new range of applications to be considered.

Zirconia bioceramic, otherwise known as yttria-tetragonal zirconia polycrystal (3Y-TZP), is currently under clinical trials to evaluate the potential for manufacture of the femoral head component in hip replacements. Coupled with high wear resistance and biocompatibility, zirconia bioceramic displays a flexural strength twice that of alumina [1, 2] and has a superior toughness. The toughness of 3Y-TZP is brought about by a stress-induced phase transformation, whereby the metastable tetragonal phase transforms under stress to a stable monoclinic phase. The associated lattice expansion produces compressive stress components at the tip of an advancing crack. Moreover, the volume expansion consumes energy that would otherwise be used to propagate a crack. As zirconia derives its toughness from the stress-induced tetragonal to monoclinic phase transformation, it is important that it has a fully tetragonal structure. Several studies [3, 4] have shown that there is a critical grain size to ensure a fully tetragonal structure. This grain size is dependent on the percentage of stabilising agent (yttria) and ranges from around 0.22 μm to 1.0 μm for yttria contents of 2% to 3%, respectively [3]. The implementation of stringent processing conditions should result in a more consistent material with low variability in strength. However, the fracture performance of all ceramic materials is governed by the size of the strength-limiting flaws. Typical failure-initiating flaws identified in ceramics [5–9] include intrinsic flaws such as agglomerates, pores and inclusions (with sizes less than around 90 μm) and machining defects with the failure stress being lower for larger defects. Accordingly, it is vital to understand the relationship between the size of the incipient flaw and the stress under which it will be exposed. Furthermore, over recent years, there has been evidence that ceramic materials are prone to the effects of fatigue [10–19]. Therefore, as many ceramic components will be exposed to cyclic stresses, it is important to understand the fatigue behaviour and to ascertain the length of time/number of cycles at a given stress necessary to grow the incipient flaw to a critical size for failure. This paper presents details of flaw analyses for both

monotonic and fatigue failures of disc-shaped specimens of zirconia bioceramic.

2. Material and experimental

The fabrication of zirconia bioceramic discs involved isostatically pressing a fine starter powder into a cylindrical green blank of diameter 45 mm. Individual discs of thickness 3 mm were sectioned from the green blank before firing whilst the material was still soft enough to be machined. However, when the cutting tool reached a critical depth of 17–18 mm, the discs fractured away from the cylindrical blank, leaving a central 'pip' of diameter 9–10 mm and protruding approximately 3 mm from the machined surface of both sides of the discs (Fig. 1). Further machining was conducted in an attempt to remove these 'pips'. Thereafter, the discs were fired to give a sintered product of 99% theoretical density. The dimensions of the discs reduced to 2 mm thickness and 36 mm diameter during densification. Dye penetration testing was then performed to identify surface defects which, if present, result in the disc specimen being rejected. However, sub-surface damage could not be identified by dye penetration and these flaws remain undetected.

Disc specimens of as-fired zirconia bioceramic were subjected to biaxial stresses in a concentric ring-loading arrangement. This apparatus is shown schematically in Fig. 2, with the dimensions of the disc specimen, loading and support rings presented in Fig. 3. According to

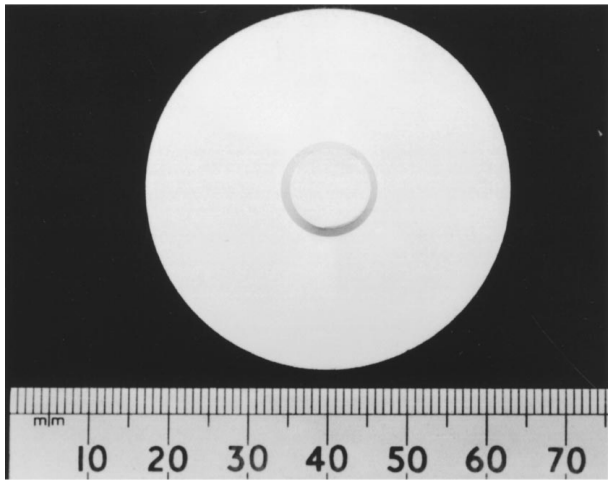

Figure 1 Green-machined 3Y-TZP disc (top view) depicting size of 'pip' remaining on the surface after fracture from the green blank.

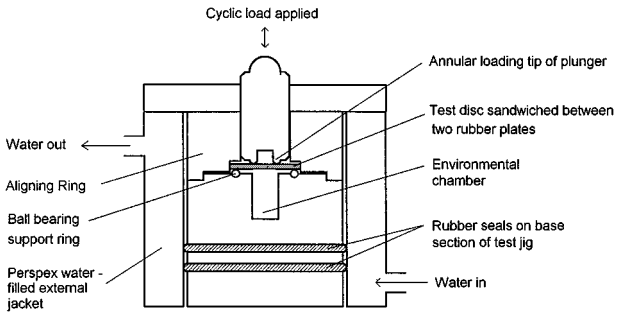

Figure 2 Concentric ring apparatus for testing disc specimens under ambient and environmental conditions.

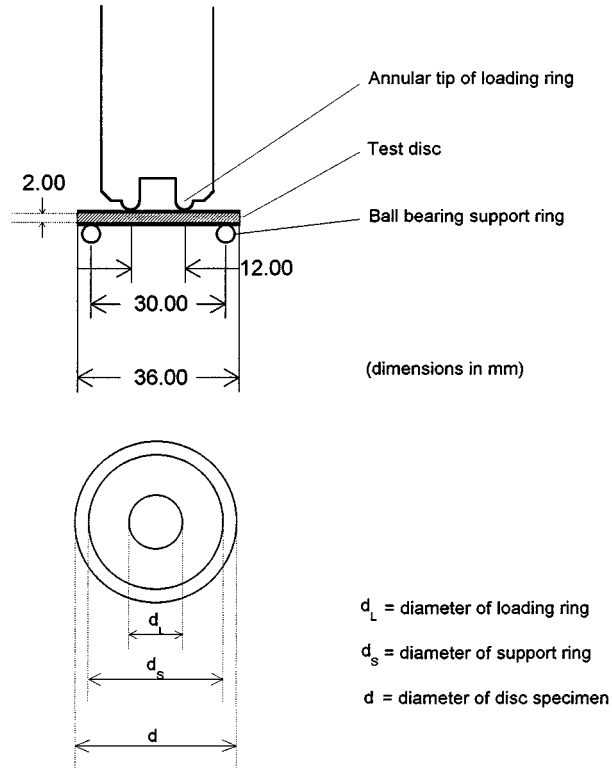

Figure 3 Schematic representation of disc specimen indicating dimensions of the disc and the diameter of the loading and support rings.

the linear plate bending theory [20], an unclamped disc loaded in such an arrangement experiences an equibiaxial stress on its tensile surface in the area below the loading ring. A detailed description of the apparatus and its mechanical performance, along with an analysis of the stresses in a concentrically loaded disc can be found elsewhere [21, 22].

Prior to loading, the dimensions of each disc were measured using a calibrated micrometer. The specimens were examined using an optical microscope in an initial attempt to identify the existence of surface flaws. In addition, as the disc specimens were only 2 mm thick, by holding them up to a high-powered light source and viewing from the opposite side, it was also possible to identify some sub-surface flaws which resulted in a scattering of the light and therefore appeared darker than the surrounding material. The position of such defects was recorded to identify whether subsequent disc failures originated here.

In the present analysis, discs were subjected to flexural strength tests and cyclic fatigue tests. In the case of discs subjected to flexural strength tests, the specimen was placed in the concentric ring apparatus with a disc of paper on the upper surface and a rubber plate (Shore hardness 60) placed on the lower surface. The apparatus was installed in a servo-hydraulic test machine and loads applied to the surface of the disc via the upper loading ring at a rate of 500 N/s under ambient conditions, so as to comply with the standard ISO 13560 [2]. The applied load and travel of the ram were recorded every 0.1 s. A trip switch, activated immediately after the test had commenced, halted the ram movement when the load on the disc had fallen to less than 0.05 kN; at this point the disc had failed. At the

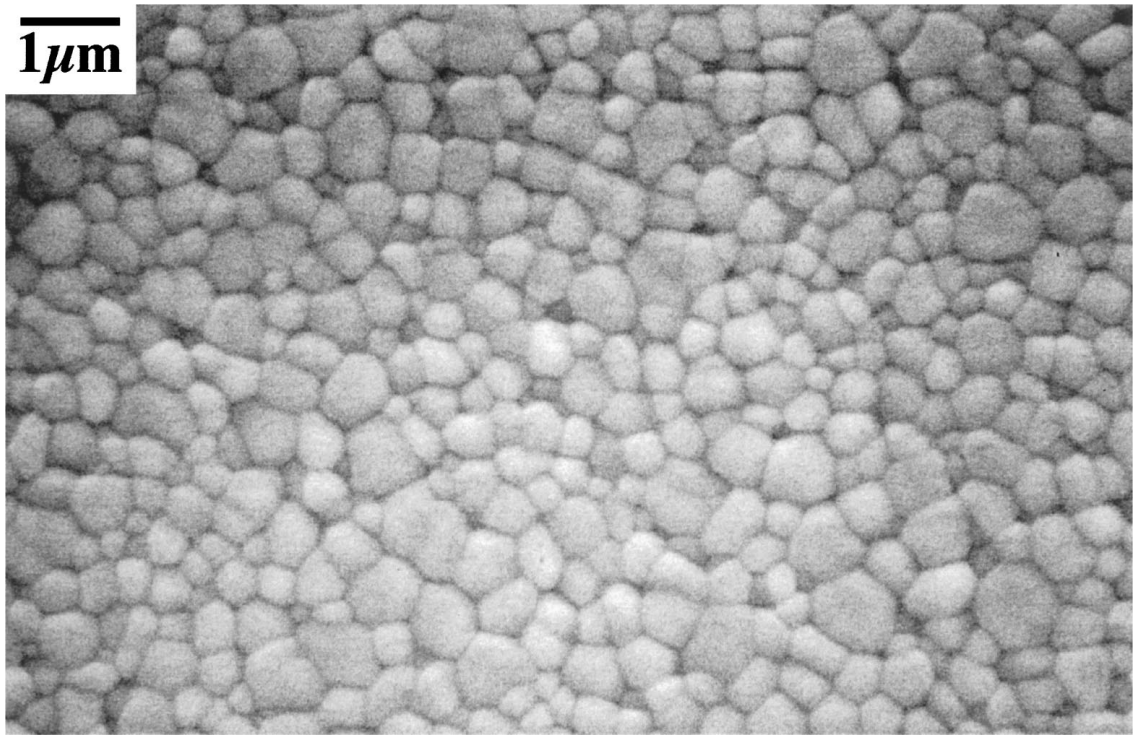

Figure 4 Micrograph of zirconia bioceramic showing a uniform grain structure with average grain size 0.46 μm.

point of failure, discs fractured into varying numbers of major fragments. Thus, by halting the ram movement at the point of failure, subsequent secondary fractures were prevented, thereby minimising the complexity of identifying the origin of failure initiation.

Discs subjected to cyclic loading conditions were tested in the same apparatus as those in the flexural strength tests at a stress ratio of $R = 0.1$ and at frequencies of 1 Hz and 5 Hz. The fatigue tests were conducted in a phosphate-buffered Ringer's solution* at 37°C to simulate the physiological conditions experienced within the body. Rubber plates sandwiched the test disc, the lower plate having a central region cut away to expose the peak stressed region of the disc to the environment. Discs were tested over a range of peak cyclic stresses and the number of cycles at the point of failure recorded, along with the peak stress. A detailed evaluation of the fatigue behaviour noted is described elsewhere [22]. The fatigue endurance behaviour has been given previously [22], with the present work considering details of fracture initiation and propagation.

The microstructure of the material was observed by grinding and polishing fragments of failed zirconia disc specimens to a smooth surface finish, followed by a thermal etch for 50 minutes at 1450°C. The material was then coated with a thin layer (a few nanometers) of gold to provide a suitably conductive layer and viewed in a scanning electron microscope (S.E.M.). Grain size measurements were conducted using the linear intercept method [23]. The typical microstructure of the thermally etched material is shown in Fig. 4.

* Ringer's solution: A colourless, aqueous solution of calcium chloride, sodium chloride and potassium chloride, buffered to a pH of 7 (20°C) and having the same osmotic pressure as blood serum.

For all disc tests, the failed specimens were reassembled to estimate the site of failure initiation. Thereafter, the appropriate fragments were examined in the S.E.M. to identify the character of the failure-initiating flaw and record information regarding crack propagation. A computer-based Image Analysis package was used to quantify surface characteristics, including accurate measurement of the exposed surface area of each failure-initiating flaw.

3. Results

Microstructural observations of the zirconia bioceramic revealed a consistent material with a fine, uniform grain size (Fig. 4), the average grain size being 0.46 μm. For all discs, failure initiated on the tensile face of the specimen within the region of the upper loading ring, i.e. the area of the disc exposed to peak tensile stresses. Discs failing at a higher stress generally fractured into a larger number of fragments than those failing at a lower stress, e.g. with failures greater than 600 MPa, at least eleven major fragments were produced, whereas for failures less than 250 MPa, discs fractured into five or less fragments. In all cases, the specimens were examined after testing to establish the location of fracture initiation. This process involved re-assembling fractured discs to evaluate the fracture pattern, thus enabling identification of the appropriate fragment possessing the initiating flaw. For high-strength disc failures (>600 MPa), flaw identification was not possible due to the high fragmentation (eleven and thirteen fragments). However, for all other failures where fragmentation was lower, the appropriate fragment possessing the initiating flaw could easily be isolated and the flaw identified by examining the fracture surface in the S.E.M.

3.1. Monotonic Failures

The data for the flexural strength tests are plotted as travel of loading ram against failure stress in Fig. 5. Two specimens failed at stresses greater than 600 MPa, with all other discs failing at stresses equal to or less than 260 MPa. In addition to discs subjected to flexural strength tests, a number of discs failed during the initial loading cycle of a fatigue test and therefore, like the flexural strength tests, failed under a monotonic load. For all monotonic failures where initiating flaws could be detected, fractographic analysis at the site of failure revealed a semi-elliptical shaped feature (Fig. 6). By measuring the surface area of these flaws (a_c^2), the relationship between failure stress and critical flaw size (a_c) could be determined. The dependence of failure stress on the size of a flaw is given by the following equation [24]:

$$K_{IC} = Y\sigma_f\sqrt{a_c} \tag{1}$$

where K_{IC} = the critical stress intensity factor (MPam$^{1/2}$), Y = a geometric shape factor for a flaw, σ_f = failure stress (MPa), and a_c = critical flaw size (m). By rearranging Equation 1, it can be seen that the failure stress is inversely proportional to the square root of the flaw size, as shown below:

$$\sigma_f = \frac{K_{IC}}{Y}\frac{1}{\sqrt{a_c}} \tag{2}$$

The monotonic disc failures were in good agreement with Equation 2, Fig. 7, i.e. the failure stress, σ_f, was inversely proportional to the square root of the flaw size, a_c. This good agreement permits a value for the critical stress intensity factor, or fracture toughness of the material (K_{IC}), to be determined from the slope, K_{IC}/Y, if the geometric shape factor, Y, is known. The value for Y was evaluated by introducing a controlled flaw into the centre of disc specimens (tensile surface)

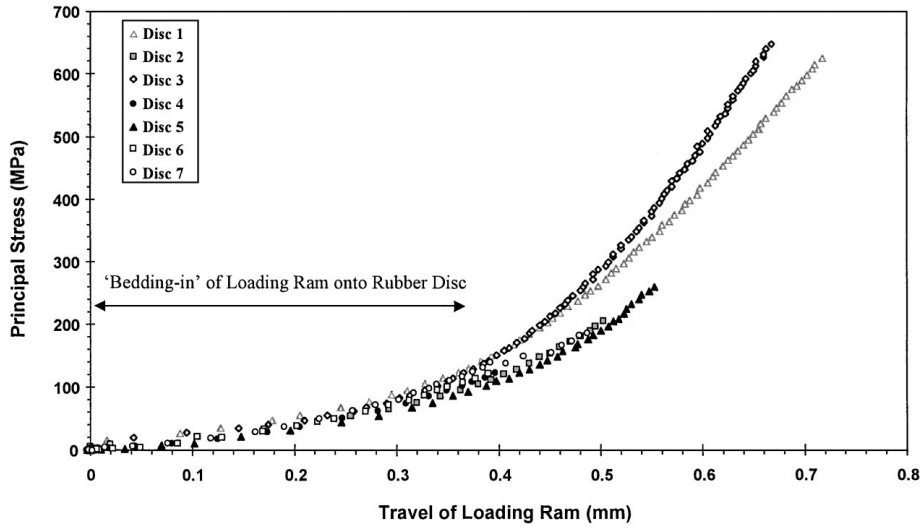

Figure 5 Flexural strength data for discs of zirconia bioceramic.

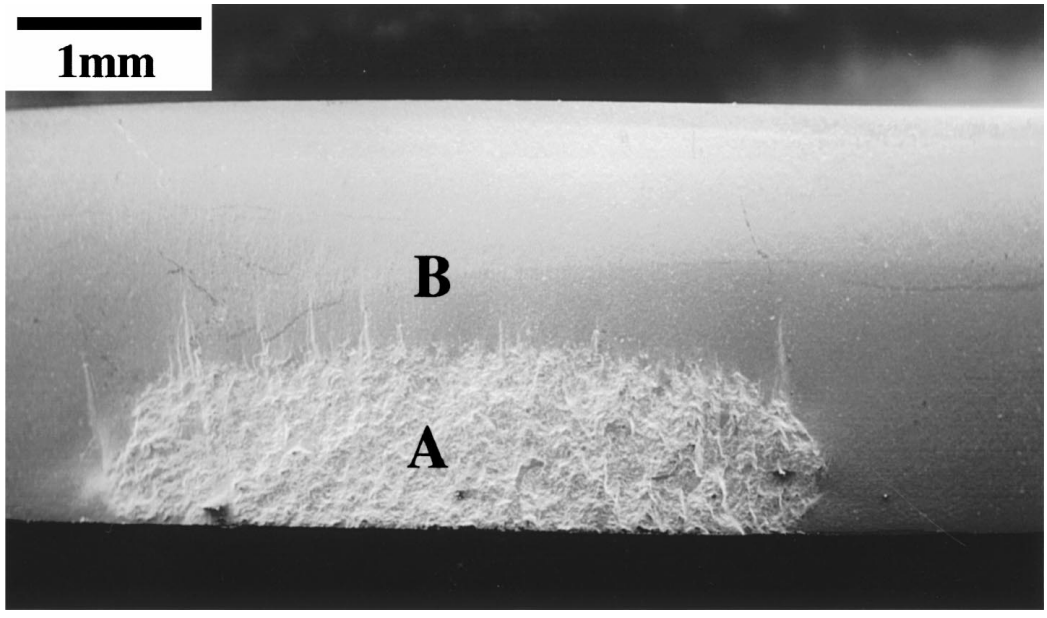

Figure 6 Fracture surface of disc failing under monotonic loading showing semi-elliptical flaw, region 'A' and area of crack propagation, region 'B'.

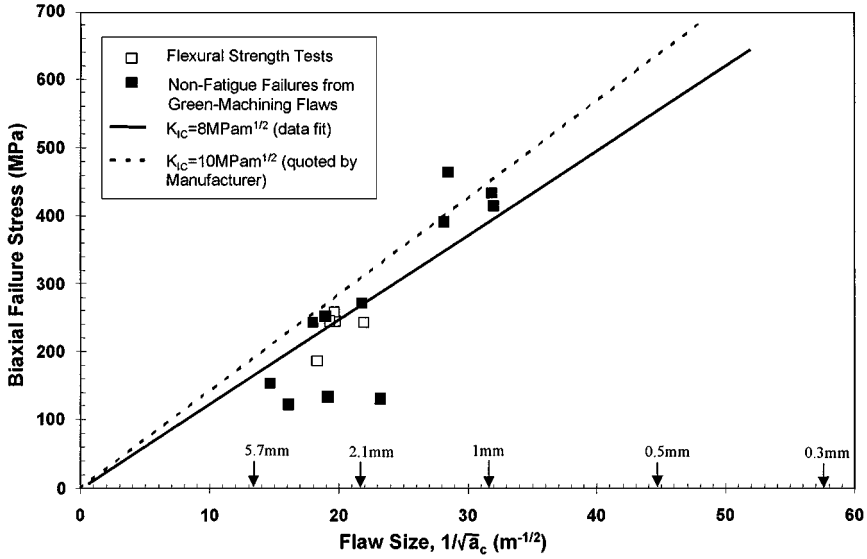

Figure 7 Relationship between critical flaw size and biaxial failure stress for zirconia bioceramic discs. The critical stress intensity factor (K_{IC},) calculated from the slope (K_{IC}/Y), is 8 MPam$^{1/2}$.

using a Vickers indenter (30 kg) and loading to failure in the concentric ring apparatus. By measuring the size of the pre-crack on the fracture surface beneath the indent and recording the failure load, the geometric shape factor could be calculated from the J integral using finite element analysis techniques. Further details of this procedure can be found elsewhere [21, 22]. The value for the geometric shape factor, Y, was determined as 0.7 ($\pm$0.01). Therefore, from the slope of Fig. 7, the fracture toughness for the material was determined as 8 MPam$^{1/2}$. This is slightly lower than the value of 10 MPam$^{1/2}$, quoted by the manufacturer. However, in the present analysis, the slope for a fracture toughness of 10 MPam$^{1/2}$ appears to be an over-estimation. Furthermore, the fracture toughness quoted for 3Y-TZP by Lui and Chen was 5.33 MPam$^{1/2}$ [5]. Accordingly, the value of 8 MPam$^{1/2}$ seems reasonable.

3.2. Fatigue failures

The results of the fatigue tests at a stress ratio of $R = 0.1$ and loading frequencies of 1 Hz and 5 Hz are presented in Fig. 8. Although there is a degree of scatter in the data, it is clear that the number of cycles achieved increased with a decrease in peak cyclic stress. Moreover, there is evidence that a fatigue limit of 450 MPa is reached at fatigue lives greater than 10^6 cycles. A number of run-outs were recorded below the fatigue limit and therefore if flaws were present, they were too small and/or the cyclic stress too low to initiate a fatigue crack.

A range of failure-initiating flaws were identified on the fracture surface of discs subjected to cyclic loading. Typical flaws identified included agglomerates or holes of agglomerate/hole pairs, inclusions, collapsed pores and machining defects. The appearance of typical defects are shown in Fig. 9a–d. Detailed examination of the fracture surface of discs failing from fatigue revealed a feint semi-elliptical demarcation line, surrounding the initiating flaw (Fig. 10). The surface area (a^2) within this region was again measured using an Image Analysis package, such that the flaw size (a) represented the critical size necessary for failure of a disc. Therefore, fatigue cracks initiated from the incipient flaw and then grew by fatigue to a critical size.

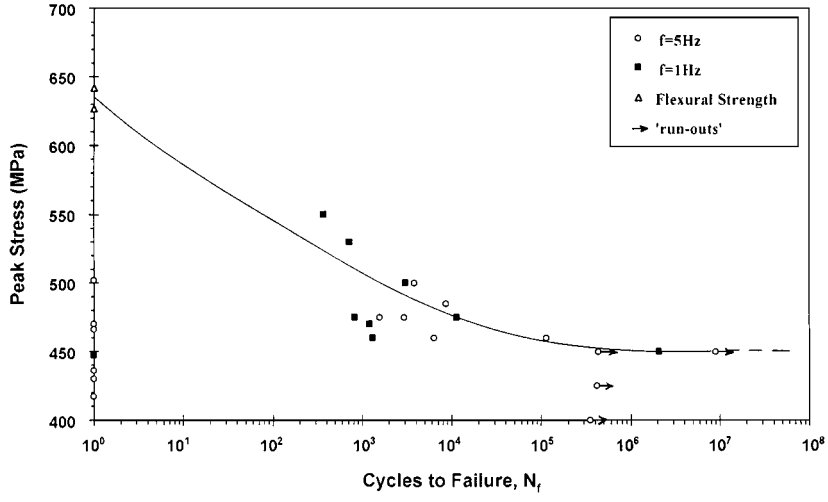

Figure 8 Cyclic fatigue curve for zirconia bioceramic discs tested in Ringer's solution at 37°C and stress ratio of R = 0.1.

Thus, the region of the fracture surface between the initiating flaw and the demarcation line represents fatigue damage.

4. Discussion and analysis of results

4.1. Monotonic failures

Two specimens subjected to flexural strength tests failed at stresses greater than 600 MPa (Fig. 5). The high energy associated with these failures resulted in major fragmentation of the disc specimens. No initiating flaws could be detected on the fracture surface of either disc due to the high fragmentation. However, the sizes of the critical flaws were estimated from the calculated fracture toughness value of 8 $MPam^{1/2}$ and the failure stress for the disc using equation 1. Thus, the calculated flaw sizes for discs failing at 627 MPa and 643 MPa were 392 μm and 374 μm, respectively. The same values for the critical flaw sizes can also be determined from Fig. 7. For all other monotonic

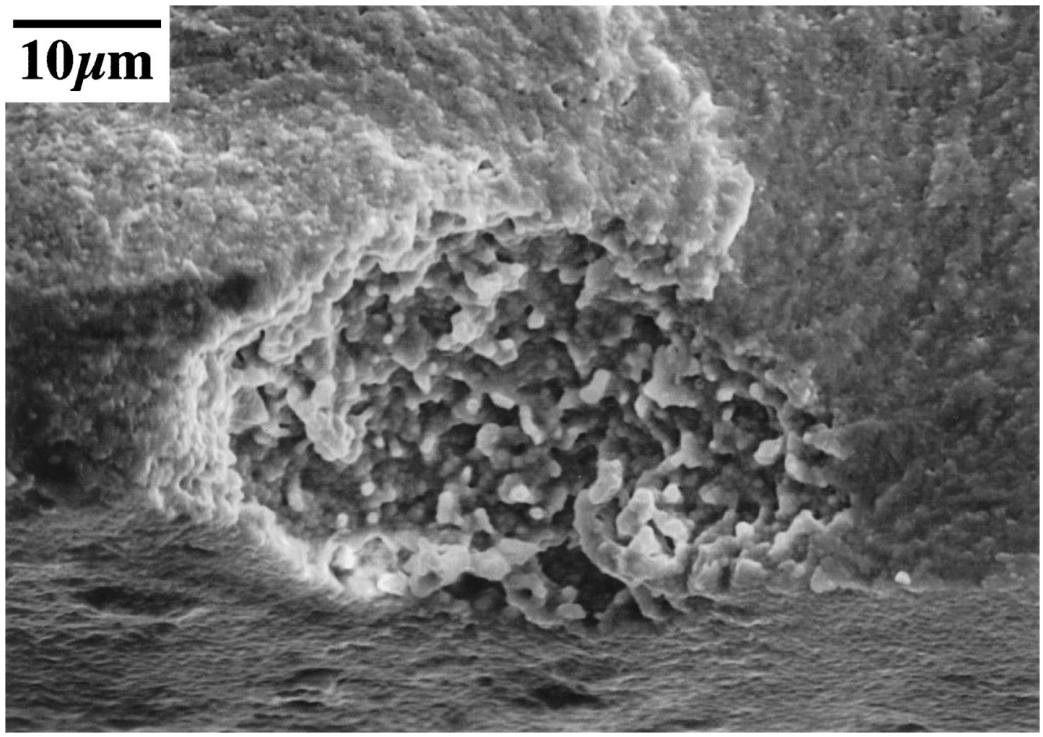

(a)

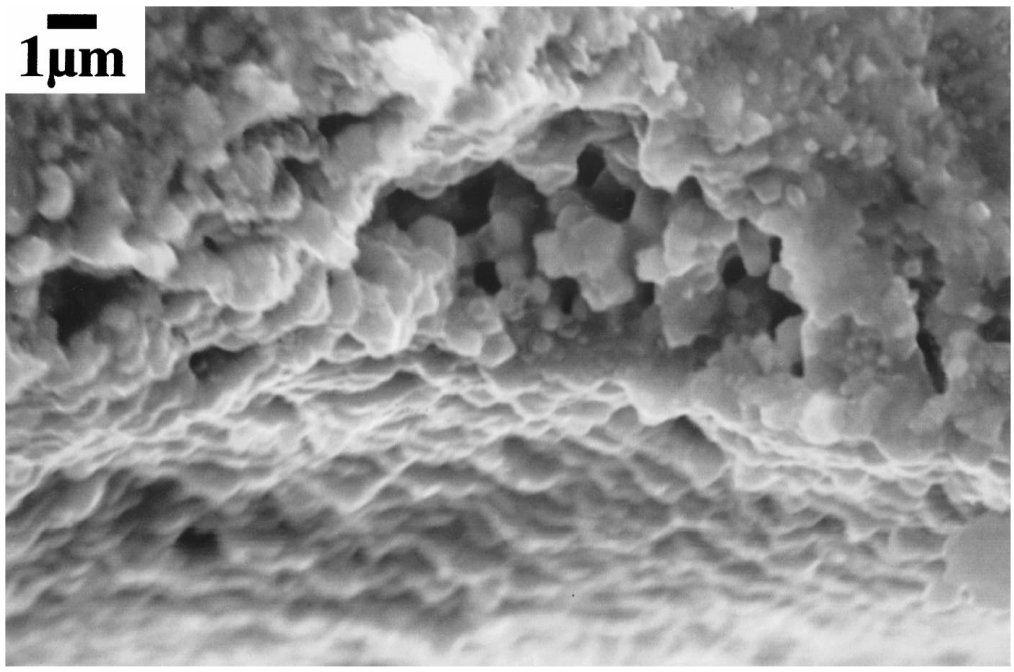

(b)

Figure 9 (a) Typical processing flaw (a hole of an agglomerate/hole pair) observed on the fracture surface of a zirconia disc specimen failing from fatigue. The flaw acted as the initiation site (surface area of flaw, a^2, is 816 μm^2). (b) Typical processing flaw (a collapsed pore) observed on the fracture surface of a zirconia disc specimen failing from fatigue. The flaw acted as the initiation site (surface area of flaw, a^2, is 197 μm^2). (c) An inclusion of alumina observed on the fracture surface of a zirconia disc specimen failing from fatigue. The flaw acted as the initiation site (surface area of flaw, a^2, is 447 μm^2). (d) A processing flaw consisting of a hole of an agglomerate/hole pair, of surface area 399 μm^2. (*Continued*)

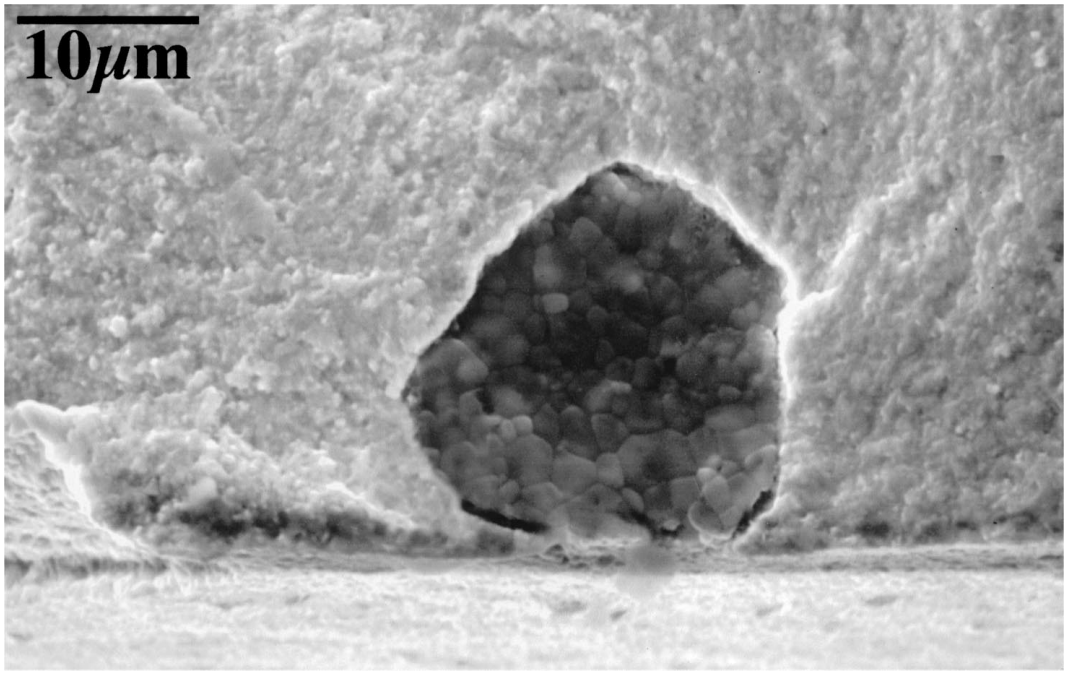

(c)

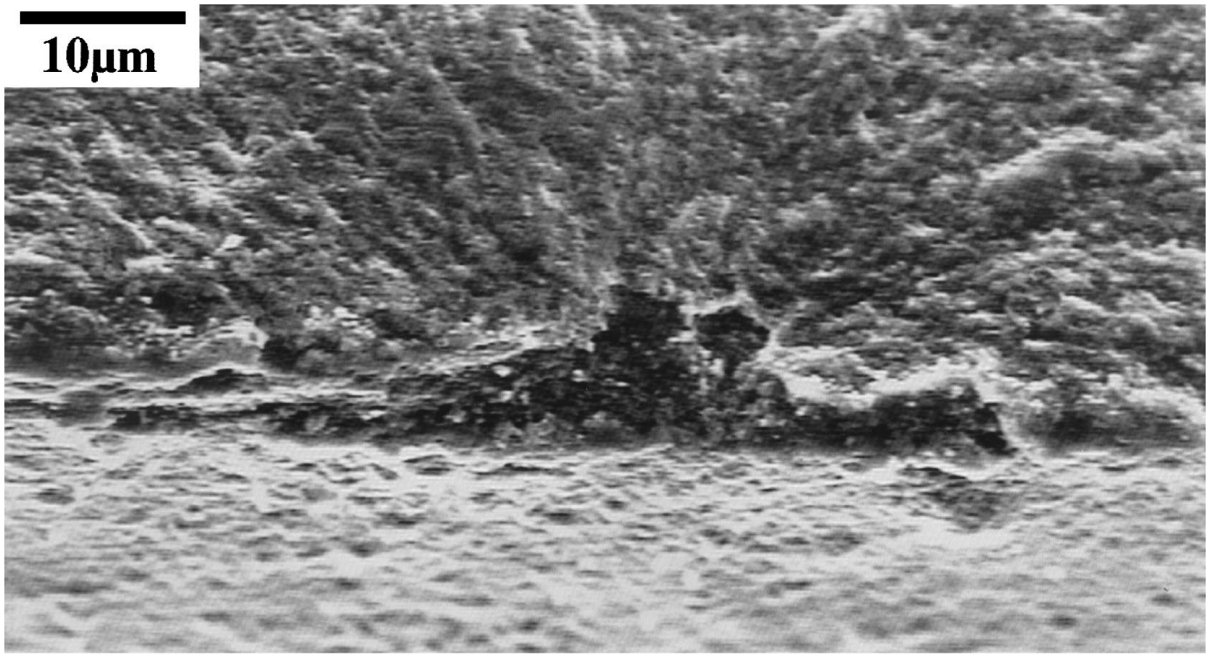

(d)

Figure 9 (*Continued*).

disc failures, the failure-initiating flaws had a semi-elliptical appearance, as depicted in Fig. 6. Such flaws are unique to ceramic disc specimens, due to the method of fabrication. Green-machine tearing occurring when the individual discs fracture away from the cylindrical blank is believed to cause the sub-surface damage depicted in Fig. 6. At higher magnification, the fracture surface differs in region 'A' (flaw) and 'B' (outside the flaw), as indicated in Fig. 11a and b, respectively. Within the vicinity of the flaw (Fig. 11a), the fracture surface has an intergranular morphology but is predominantly transgranular outside this region. Although the green-machine tearing is likely to have occurred on both faces of the disc specimens, examination of the fracture surface (Fig. 6) might indicate that the damage only occurred on one face. However, the semi-elliptical nature of the flaw is due to the manner in which the discs were loaded and is common for all specimens loaded in flexure.

4.2. Fatigue failures

The data given in Fig. 8 clearly show that zirconia bioceramic is prone to the effects of fatigue. Although some researchers have observed fatigue striations on the fracture surface of ceramic materials [25], no such features were observed in the present analysis. In all cases, the fracture-initiating flaw was on or connected to the tensile surface of the disc. However, in the case of discs that had undergone fatigue failures, the feint

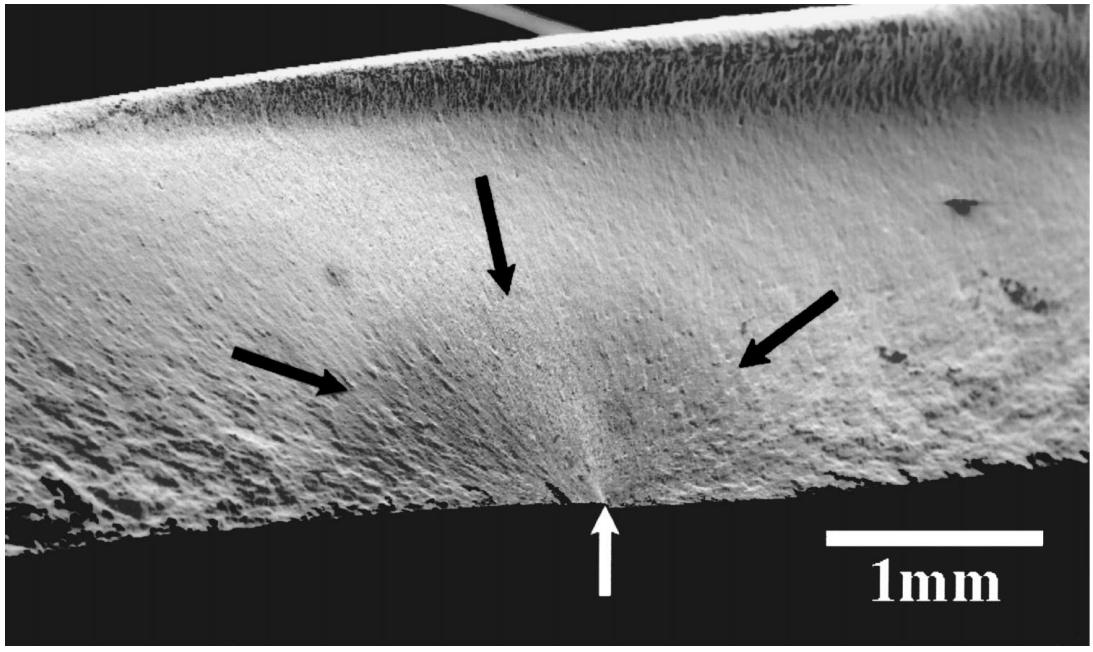

Figure 10 Fracture surface of a zirconia disc specimen failing from fatigue, depicting the extent of fatigue crack growth (indicated by dark arrows), initiated from a pre-existing flaw at the point indicated by the white arrow. The surface area of fatigue damage is 0.489 mm^2, originating from a flaw of surface area 816 μm^2.

demarcation line surrounding the initiating flaw (Fig. 10) suggested that some fatigue crack growth had occurred. Therefore, fatigue cracks initiated from the pre-existing flaw and grew by fatigue to a critical size for failure. Hence, the fracture surface between the initiating flaw and the line of demarcation represents damage due to fatigue crack growth. Outside this region, fracture occurred due to overload.

The information given in Fig. 7 enables the critical flaw size at a given stress to be determined. Therefore, if an incipient flaw is of a critical size at the applied stress, the specimen will fail under monotonic loading. However, if the flaw is smaller than the critical size for a given stress, the disc specimen will only fail when the area of damage accumulates under cyclic loading to the critical size for failure. This critical size is the same for a given stress but a greater number of fatigue cycles will accumulate as the size of incipient flaw decreases.

With both the initiating and critical flaw sizes determined and the number of cycles taken to grow the flaw to the critical size recorded, it is possible to calculate the average fatigue crack growth rate. The crack growth rate generally increased with peak cyclic stress, with growth rates at 550 MPa being around 1×10^{-5} cycles/second and falling to around 9×10^{-7} cycles/second at a peak cyclic stress of 475 MPa. Determination of the critical flaw size, and hence the average crack growth rate, should therefore be possible for all specimens, provided the initiating flaw size is known. Under the same test conditions, for any disc cycled at the same peak stress, the resulting critical flaw size should be the same, and fracture surface analysis revealed that this was indeed the case.

By subjecting disc specimens to cyclic loading under constant peak biaxial stress conditions, it was possible to determine the relationship between the fatigue life of the discs and the size of the initiating flaw, measured from the fracture surface. The relationship between flaw size and fatigue life is given in Equation 3 [26]:

$$N_f = \frac{2}{C(m-2)Y^m \Delta\sigma^m}\left[\frac{1}{a_i^{(m-2)/2}} - \frac{1}{a_c^{(m-2)/2}}\right] \quad (3)$$

where N_f = cycles to failure, C = a material constant, m = crack growth exponent (equivalent to Paris crack growth slope) [27], $\Delta\sigma$ = stress range, Y = geometric flaw shape factor, a_i = incipient flaw size, and a_c = critical flaw size. For a given stress range, $\Delta\sigma$, the term $2/C(m-2)Y^m\Delta\sigma^m$ is a constant, A′. The value of m is also constant for the same material when testing under identical environmental conditions and is generally high (20–40) for ceramic materials [e.g. 25, 28]. As the value of m is high, the term $1/a_c^{(m-2)/2}$ is negligible compared with $1/a_i^{(m-2)/2}$. Therefore, Equation 3 thus reduces to

$$N_f = A'\left[\frac{1}{a_i^{(m-2)/2}}\right] \quad (4)$$

and in logarithmic form becomes

$$\log N_f = -[(m-2)/2]\log a_i + \log A' \quad (5)$$

From Equation 5, data were plotted for three constant peak biaxial stress conditions (Fig. 12) and shows that there is a linear relationship for the logarithmic plot of cycles to failure against initiating flaw size. As expected, for each peak stress condition, the number of cycles to failure decreases as the initiating flaw size increases and the fatigue life decreases with increasing peak cyclic stress. From the plot, the gradient, $-[(m-2)/2]$ was measured as -9, giving an m value of 20. This is quite reasonable and agrees with published values for ceramic materials [5, 28, 29].

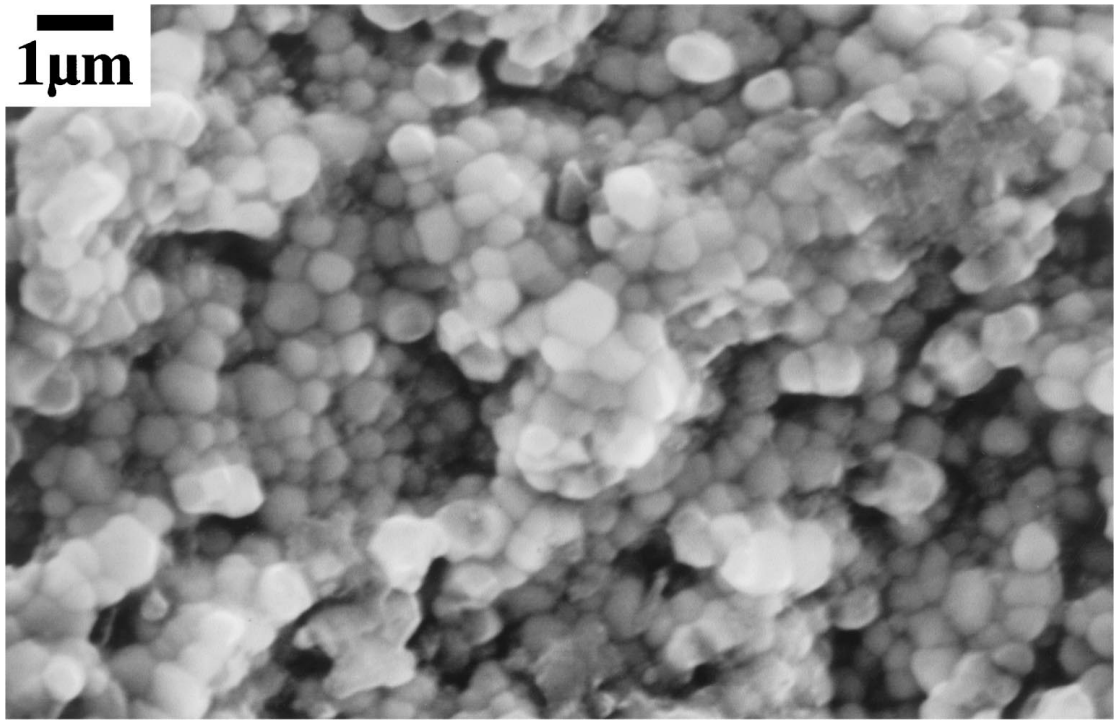

(a)

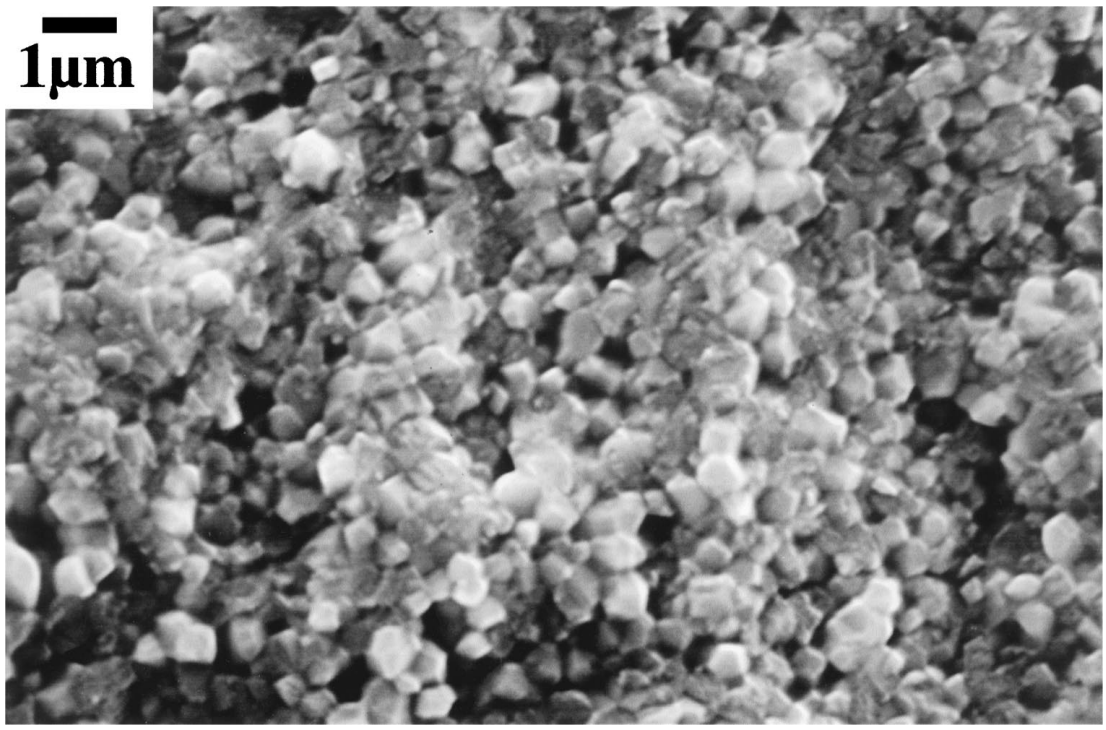

(b)

Figure 11 (a) Fracture surface of a disc in region 'A' of Fig. 6. The damage due to green-machine tearing has resulted in an intergranular fracture surface morphology. (b) Fracture surface of a disc in region 'B' of Fig. 6. This area of the fracture surface is outside the semi-elliptical shaped flaw and has a predominantly transgranular morphology.

From Fig. 12, the fatigue life for a range of initiating flaw sizes is obtained. Thus, Fig. 13 displays fatigue curves for initiating flaw sizes of 10 μm, 15 μm, 20 μm and 30 μm. In addition to the constant flaw size fatigue curves, four examples of measured flaw sizes are highlighted on the plot with micrographs of each flaw given in Fig. 9a–9d. The measured flaws indicated in Fig. 9a and c at 485 MPa and 550 MPa respectively, are expected to lie close to the constant flaw size slopes as they were used in the slope construction. However, it is interesting to see that flaw sizes at a peak stress of 500 MPa, which were not used in the slope construction, also fit remarkably well with the rest of the data. Thus, a disc cycled at a peak stress of 500 MPa failed from fatigue after 6×10^4 cycles from a collapsed pore (Fig. 9b). The size of this initiating flaw was 14 μm. Another

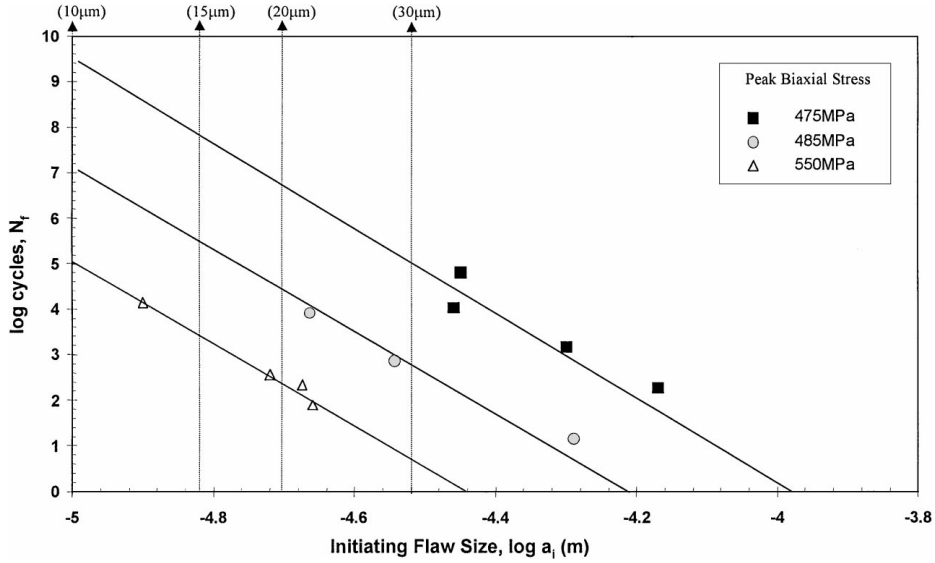

Figure 12 Relationship between initiating flaw size and fatigue life of zirconia bioceramic discs under constant peak biaxial stress conditions.

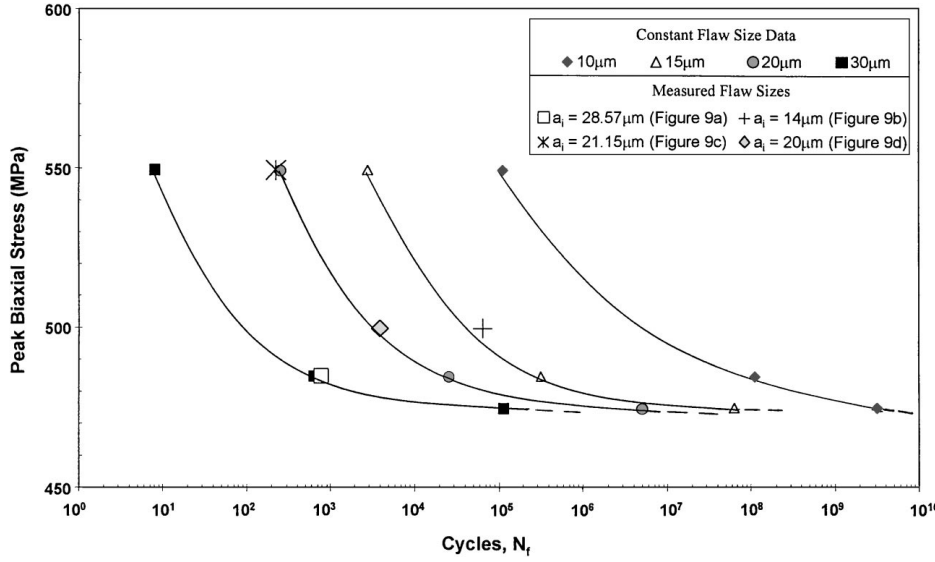

Figure 13 Constant flaw size fatigue curves for zirconia bioceramic discs, derived from Fig. 12. A range of measured incipient flaw sizes for discs of given fatigue life are also included for comparison.

disc cycled at 500 MPa failed after almost 4×10^3 cycles from an agglomerate with an initiating flaw size of 20 μm (Fig. 9d). Both these measured flaw sizes lie extremely close to the constant flaw size fatigue slopes of 15 μm and 20 μm. It is possible therefore to estimate the size of the initiating flaw, based on the constant flaw size fatigue data. Furthermore, if the initiating flaw size is known, it may be possible to estimate the expected fatigue life of a disc specimen at a given peak cyclic stress.

It should be emphasised, however, that whilst a similar procedure could be conducted for different materials and specimen geometry, the present study is only applicable to 3Y-TZP discs exposed to an equibiaxial stress field. Moreover, it is important to note that the flaws measured from the fracture surface are only two-dimensional and therefore the size of the flaw was determined from the exposed surface area and not the volume of the flaw. Nevertheless, as all flaws were measured in the same way, the study provides a suitable method for predicting the likely mechanical performance of 3Y-TZP discs.

5. Concluding remarks

The results for zirconia disc specimens failing under monotonic loads clearly show that there is a linear relationship between the size of the incipient flaw and failure stress. The critical stress intensity factor, or fracture toughness, determined from the slope was 8 MPam$^{1/2}$. For discs undergoing fatigue cycles, the critical stress intensity factor was not achieved until sufficient crack growth had occurred. At this point, the damage was of a sufficient size to result in disc failure. Under the present test conditions, it was possible to predict the critical flaw size necessary for failure of discs under fatigue loading. The predicted size was the same or very similar to that measured from the fracture surface. Predictive constant flaw size fatigue curves enabled an estimation of the size of the initiating flaws for discs

failing from fatigue. The predicted values were close to the true flaw size, measured from the fracture surface of failed disc specimens. The crack growth exponent, m, was determined as 20 which is similar to that established for other ceramic materials using crack growth techniques on notched specimens.

References

1. ISO standard—Implants in Surgery: Ceramic Materials Based on Alumina, ISO 6474 (1994)/BS 7253 Pt. 2 (1997).
2. ISO standard—Implants in Surgery: Ceramic Materials Based on Yttria Stabilised Zirconia, ISO 13560 (1997)/BS 7253 Pt. 6 (1997).
3. F. F. LANGE, *J. Mat. Sci.* **17** (1982) 240.
4. M. J. READEY and MCCALLEN, *J. Amer. Ceram. Soc.* **78**(10) (1995) 2769.
5. S. LIU and I. CHEN, *ibid.* **74**(6) (1991) 1197.
6. M. OISHI, Y. MATSUDA, K. NOGUCHI and T. MASAKI, *ibid.* **78**(5) (1995) 1212.
7. L. CHAO and D. SHETTY, *ibid.* **74**(2) (1991) 333.
8. K. NOGUCHI, Y. MATSUDA, M. OISHI, T. MASAKI, S. NAKAYAMA and M. MIZUSHINA, *ibid.* **73**(9) (1990) 2667.
9. Military Handbook, "Fractography and Characterization of Fracture Origins in Advanced Structural Ceramics", MIL—HDBK—790, Department of Defence, United States of America (July 1991).
10. R. H. DAUSKARDT, W. YU and R. O. RICHIE, *J. Amer. Ceram. Soc.* **70**(10) (1987) C248.
11. R. H. DAUSKARDT, D. B. MARSHALL and R. O. RICHIE, *ibid.* **73**(4) (1990) 893.
12. R. H. DAUSKARDT, W. C. CARTER, D. K. VEIRS and R. O. RICHIE, *Acta Metall. Mater.* **38**(11) (1990) 2327.
13. R. H. DAUSKARDT, M. R. JAMES, J. R. PORTER and R. O. RICHIE, *J. Amer. Ceram. Soc.* **75**(4) (1992) 759.
14. S. HORIBE, *J. Mat. Sci. Lett.* **7** (1988) 725.
15. S. HORIBE and R. HIRAHARA, *Acta Metall. Mater.* **39**(6) (1991) 1309.
16. A. UENO, H. KISHIMOTO, H. KAWAMOTO and M. ASAKURA, *Engng. Fract. Mech.* **40**(4/5) (1994) 1153.
17. D. S. JACOBS and I. W. CHEN, *J. Amer. Ceram. Soc.* **77**(5) (1994) 1153.
18. F. GUIU, *J. Mat. Sci. Lett.* **13** (1978) 1357.
19. D. A. J. VAUGHAN, PhD thesis, Queen Mary and Westfield College, University of London 1989.
20. E. J. HEARN, "Mechanics of Materials" Vol. 2, (Pergammon Press plc., Oxford, 1985) p. 636.
21. B. J. HULM. J. D. PARKER and W. J. EVANS, *J. Mat. Sci* **33** (1998) 3255.
22. B. J. HULM, PhD thesis, University of Wales, Swansea 1998.
23. Standard Test Method for Determining Average Grain Size, ASTM E112-88 (1988).
24. T. L. ANDERSON, "Fracture Mechanics: Fundamentals and Applications" 2nd ed. (CRC Press Inc., Boca Raton, Florida, 1995) ch. 2.
25. S. LIU and I. CHEN, *J. Amer. Ceram. Soc.* **74**(6) 1206.
26. T. L. ANDERSON, "Fracture Mechanics: Fundamentals and Applications" 2nd ed. P520 (CRC Press Inc., Boca Raton, Florida, 1995).
27. P. C. PARIS and ERDOGAN, *J. Basic Eng. Trans.* ASME **85** (1963) 528.
28. C. J. GILBERT, R. H. DAUSKARDT and R. O. RICHIE, *J. Amer. Ceram. Soc.* **78**(9) (1995) 2291.
29. R. H. DAUSKARDT and R. O. RICHIE, *Closed Loop* **17**(2) (1995).

Received 28 June
and accepted 19 August 1999